Alternative determinism principle for topological analysis of chaos

Marc Lefranc

*Laboratoire de Physique des Lasers, Atomes, Molécules, UMR CNRS 8523, Centre d'Études et de Recherches Lasers et Applications,
Université des Sciences et Technologies de Lille, F-59655 Villeneuve d'Ascq, France*
(Received 7 December 2004; revised manuscript received 9 August 2006; published 13 September 2006)

The topological analysis of chaos based on a knot-theoretic characterization of unstable periodic orbits has proven to be a powerful method, however knot theory can only be applied to three-dimensional systems. Still, the core principles upon which this approach is built—determinism and continuity—apply in any dimension. We propose an alternative framework in which these principles are enforced on triangulated surfaces rather than curves, and we show that in dimension 3 our approach numerically predicts the correct topological entropies for periodic orbits of the horseshoe map.

PACS number(s): 05.45.Ac, 02.10.Kn, 02.40.Sf

Chaotic behavior results from the interplay of two geometrical processes in state space: *stretching* separates neighboring trajectories while *squeezing* maintains the flow within a bounded region [1,2]. A topological analysis has been developed to classify the ways in which stretching and squeezing can organize a chaotic attractor [2–4]. It relies on a theorem stating that unstable periodic orbits (UPO) of a chaotic three-dimensional (3D) flow can be projected onto a 2D branched manifold (a *template*) without modifying their knot invariants [5]. In this method, UPO extracted from an experimental time series are characterized by the simplest template compatible with their topological invariants [2–4].

However, this approach can only be applied to 3D attractors: in higher dimensions, all knots can be deformed into each other. Although other topological methods are applicable to higher dimensions [6,7], extending template analysis is still desirable because it provides a different information. A first step to overcome the 3D limitation is to recognize that knot theory is not a necessary ingredient but simply a convenient way to study how two fundamental properties, determinism and continuity, constrain trajectories in phase space. It is because two trajectories cannot intersect that the knot type of a 3D periodic orbit is well defined and is not modified as the orbit is deformed under control parameter variation.

In this paper, we note that a dimension-independent formulation of determinism is orientation preservation, and we propose an approach in which it is enforced on a representation of the dynamics in a triangulation of periodic points. In dimension 3, an explicit formalism is easily constructed, and we find that it numerically predicts the correct entropies for periodic orbits of the horseshoe map. The entropy of a periodic orbit is an invariant defined as the minimal topological entropy [8] of a flow containing this orbit [9,10]; a positive-entropy orbit is a powerful indicator of chaos [4,11,12]. This result suggests that a key ingredient for constructing a knotless template analysis has been captured, although a proof of validity and an explicit higher-dimensional extension are still lacking.

We now detail our approach. The first step is to replace the requirement of nonintersecting curves by a geometrical problem that adapts naturally to phase spaces of any dimension. It has been suggested to exploit the rigid structure of invariant manifolds of UPO [4,13]. Here, we note that when

a volume element V of a d-dimensional phase space is advected by a deterministic flow Φ_t, the image $\Phi_t(\partial V)$ of its boundary cannot display self-intersections: at any time t, its interior and its exterior remain distinct, as with a droplet in a fluid flow. A technical formulation of this property is that volume orientation is preserved by the dynamics. For simplicity, we consider attractors embedded in $\mathbb{R}^n \times S^1$ (e.g., forced systems), which can be sliced into n-dimensional Poincaré sections parametrized by $\varphi \in S^1$. Determinism then imposes that boundaries of n-dimensional volume elements of Poincaré sections retain their orientation (Fig. 1).

Template analysis must be applicable to UPO extracted from experimental signals, and thus can only rely on the phase-space trajectory of a period-p orbit. Thus, we represent the dynamics in a triangulated space whose nodes are p periodic points P_i in a Poincaré section, with $P_{i+1}=F(P_i)$, F being the return map. In this space, points P_i are 0-cells, line segments $\langle P_i, P_j \rangle \equiv \langle ij \rangle$ joining two points are 1-cells, triangles $\langle P_i, P_j, P_k \rangle \equiv \langle ijk \rangle$ are 2-cells, etc. [Fig. 2(a)]. Similar concepts have been used in [14] to analyze the static structure of an attractor, but we focus here on the dynamics. We denote by S_m the set of collections of contiguous m-cells, which are the analogs of m-dimensional surfaces in the original phase space. As Poincaré sections are swept, periodic points move in the section plane and so do the m-cells attached to them [Fig. 2(b)]. The dynamics induced in S_m should reflect that of m-dimensional phase-space surfaces under action of the chaotic flow, and in particular should be organized by the same stretching and squeezing mechanisms.

A dynamics in the triangulated space is specified by maps $F_m:S_m \rightarrow S_m$ acting on collections of contiguous m-cells. Since the original return map F sends nodes to nodes but not
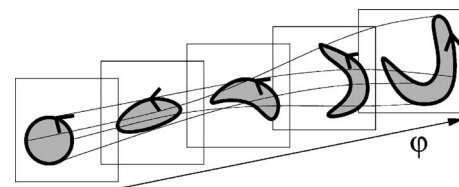

FIG. 1. Under the action of the flow, volume elements of Poincaré sections and their boundaries are stretched and squeezed but retain their orientation, as illustrated here for 2D section planes.
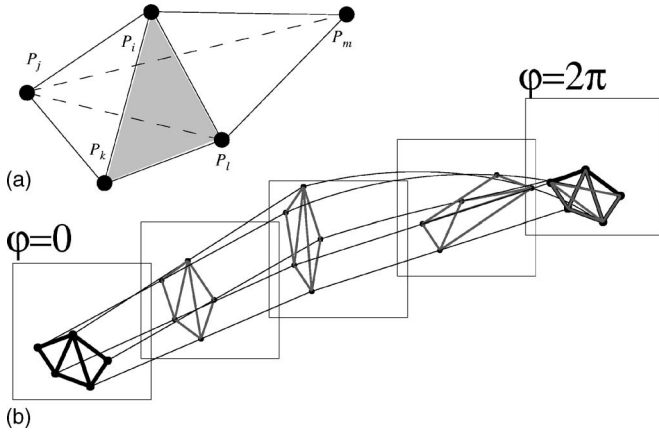
FIG. 2. (a) Triangulated space based on periodic points P_i in a 3D Poincaré section. The 2-cell $\langle ikl \rangle$ is shaded. (b) The flow induces a mapping of this triangulated space into itself, as suggested here for a period-5 orbit embedded in $\mathbb{R}^2 \times S^1$.

facets to facets, the F_m are not restrictions of F for $m > 0$. However, we require them to mimic F in the following way: they should be invertible, satisfy determinism, and result from a continuous deformation of facets, just as F is a continuous deformation of identity. The F_m should also satisfy $\partial F_m(\Sigma) = F_{m-1}(\partial \Sigma)$, where ∂ is the boundary operator. As we see below, facets are not necessarily trivially advected between sections because degeneracies occur, at which action must be taken to preserve orientation.

We now specialize to the 3D case. The volume element of a triangulated set of periodic points in a 2D Poincaré section is a triangle (2-cell) based on three periodic points P_i, P_j, and P_k. Let $P_i(\varphi)$ be the position of P_i in section φ, with $P_i(0) = P_i$ and $P_i(2\pi) = P_{i+1}$. The natural evolution of $T = \langle P_i, P_j, P_k \rangle$ as φ increases is

$$T(\varphi) = \langle P_i(\varphi), P_j(\varphi), P_k(\varphi) \rangle, \tag{1}$$

which would lead to a trivial induced return map $F_2(T) = T(2\pi) = \langle P_{i+1}, P_{j+1}, P_{k+1} \rangle$ if expression (1) were uniformly valid as a 2-cell. However, it is common that at some $\varphi = \varphi_0$, one of the three points [say $P_k(\varphi)$] passes between the two others, thereby changing the orientation of the candidate 2-cell $T(\varphi)$ given by expression (1) (Fig. 3). As emphasized above, this is strictly forbidden by determinism, and we must thus modify the representation of the dynamics. It turns out that this problem has a simple solution.

The degenerate triangle $T(\varphi_0)$ in Fig. 3 is like a flattened balloon whose boundary splits into two superimposed sides with opposing outer normals. Determinism is violated when
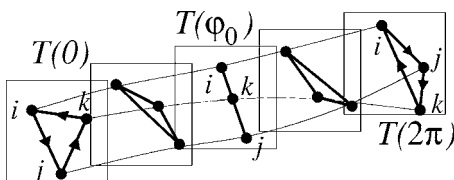

FIG. 3. As three points move in the section plane when φ is increased, the triangle they form can change its orientation.
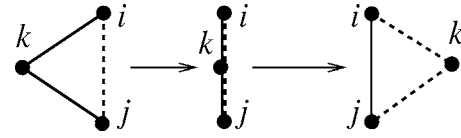

FIG. 4. A triangle is inverted as P_k passes between P_i and P_j. Identifying the solid (dashed) paths in the initial and end configurations leads to substitution (2).

these two sides cross each other so that interior and exterior, defined with respect to outer normal, seem to be exchanged. However, the experimental data only constrain node motion, from which the facet dynamics is interpolated. To preserve determinism, we force the two opposing sides not to cross by swapping them at degeneracy, thereby canceling the inversion.

This prescription is illustrated in Fig. 4, where the two opposing sides at triangle degeneracy are represented as a solid and a dashed line. The key point is that we construct the edge dynamics so that the left (solid line) and right (dashed line) sides remain at the left and right, respectively. Since the left (right) side consists of itinerary $\langle ik \rangle + \langle kj \rangle$ ($\langle ij \rangle$) before degeneracy and of itinerary $\langle ij \rangle$ ($\langle ik \rangle + \langle kj \rangle$) after degeneracy, their relative position is preserved by applying the following dynamical rule in $S_1 = S_{n-1}$ at triangle inversion:

$$\langle ij \rangle \rightarrow \langle ik \rangle + \langle kj \rangle, \tag{2a}$$

$$\langle ik \rangle + \langle kj \rangle \rightarrow \langle ij \rangle. \tag{2b}$$

These rules also apply to reverse paths (e.g., $\langle ji \rangle \rightarrow \langle jk \rangle + \langle ki \rangle$). Note that $\partial T = \partial \langle ijk \rangle = \langle ij \rangle + (\langle jk \rangle + \langle ki \rangle)$ is mapped by (2) to $(\langle ik \rangle + \langle kj \rangle) + \langle ji \rangle = \partial \langle ikj \rangle$. The permutation compensates for triangle inversion so that orientation of ∂T, and hence determinism, is preserved.

Itineraries visiting edges $e_{ij} = \langle ij \rangle$ in a given order are represented by words in a language $\mathcal{A}^*$ over alphabet $\mathcal{A} = \{e_{lm}\}$, and (2) by an operator σ_{ij}^k that in each word w replaces the letter e_{ij} by the string $e_{ik} e_{kj}$ and $e_{ik} e_{kj}$ by e_{ij} [hence $(\sigma_{ij}^k)^2 = 1$]. For example,

$$\sigma_{ij}^k e_{kl} e_{li} e_{ij} e_{jl} e_{li} \overline{e_{ik} e_{kj}} \overline{e_{ji}} \cdots = e_{kl} e_{li} \overline{e_{ik} e_{kj}} e_{jl} e_{li} \underline{e_{ij}} e_{jk} e_{ki} \cdots.$$

The σ_{ij}^k generate a nontrivial dynamics, as the image of an itinerary depends on how periodic points rotate around each other. This simple dynamics faithfully reflects that of the flow around the periodic orbit, as we show by computing the entropy of the orbit.

From the motion of periodic points $P_i(\varphi)$ in the section plane as φ is swept, a list of l triangle inversions $\sigma_{i_m j_m}^{k_m}$ is obtained, from which we build an induced return map that transforms a word $w \in \mathcal{A}^*$ into another word w' as

$$F_1 : w \rightarrow w' = N \sigma_{i_l j_l}^{k_l} \cdots \sigma_{i_2 j_2}^{k_2} \sigma_{i_1 j_1}^{k_1} w, \tag{3}$$

where $N e_{ij} \cdots = e_{(i+1)(j+1)} \cdots$. Consider periodic orbit 00111 of a suspension of the standard horseshoe map equipped with the usual symbolic coding [2] [Figs. 2(b) and 5(a)]. We find that as points gradually move in the section plane from their initial location to that of their image under the return map,
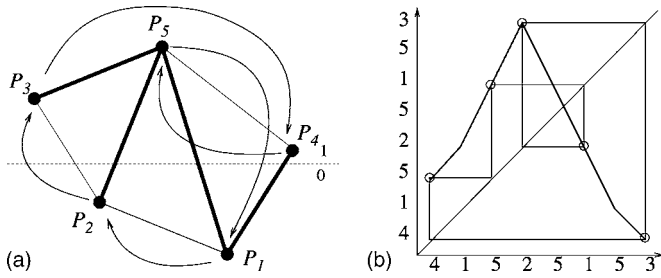
FIG. 5. (a) Periodic points of the horseshoe orbit 00111 and their schematic trajectory in section plane. Bold lines indicate edges involved in (4). (b) Path $P_4P_1P_5P_2P_5P_1P_5P_3$ folds onto itself under action of induced return map F_1. The unimodal map obtained has 00111 as a periodic orbit.

triangle inversions occur when point 4 successively crosses the four edges e_{15}, e_{13}, e_{25}, and e_{23}. Thus the induced return map for edge itineraries is $F_1 = N\sigma_{23}^4\sigma_{25}^4\sigma_{13}^4\sigma_{15}^4$. For example,

$$e_{15} \xrightarrow{\sigma_{15}^4} e_{14}e_{45} \xrightarrow{\cdots} e_{14}e_{45} \xrightarrow{N} e_{25}e_{51} = F_1(e_{15}),$$

while edges not crossed by point 4 are trivially modified (e.g., $e_{14} \xrightarrow{N} e_{25}$). This leads to the closed rule set

$$e_{14} \rightarrow e_{25}, \ e_{15} \rightarrow e_{25}e_{51}, \ e_{25} \rightarrow e_{35}e_{51}, \ e_{35} \rightarrow e_{41} \qquad (4)$$

for edges in the invariant set of F_1. Table I displays iterates $F_1^m(e_{15})$ computed using (4). Their length $|F_1^m(w)|$ diverges exponentially as $m \rightarrow \infty$, indicating that trajectories in the neighborhood of the orbit are continuously stretched apart by the flow. The growth rate

$$h(P) = \lim_{m \rightarrow \infty} \frac{\ln|F_1^m(w)|}{m} \qquad (5)$$

is obtained as the logarithm of the leading eigenvalue of the transition matrix $(M_{ee'})$, whose entries count occurrences of edge e' or of its reverse in $F_1(e)$ given by (4). Here, $h(00111) \sim 0.5435$. Table I also shows that $F_1^{kp}(w)$ (p is the orbit period) converges to an infinite word w_∞ satisfying

TABLE I. A few iterates $F_1^m(e_{15})$ are given by their itinerary between periodic points [e.g., (35152) denotes the path $e_{35}e_{51}e_{15}e_{52}$].

m	Itinerary of $F_1^m(e_{15})$
0	(15)
1	(251)
2	(35152)
3	(41525153)
4	(5251535152514)
5	(1535152514152515351525)
6	(25141525153515252515351525141525515351)
10	(153515251415251535152525153515252515351⋯)
15	(153515251415251535152525153515252515351⋯)
100	(153515251415251535152525153515252515351⋯)

TABLE II. Topological entropies of positive-entropy horseshoe orbits up to period 8 obtained with the approach described here and with the train-track algorithm (TTA).

Orbit	This work	TTA	Orbit	This work	TTA
01101 $_1^0$1	0.4421	0.4421	00010 $_1^0$1	0.3822	0.3822
001011 $_1^0$1	0.3460	0.3460	000101 $_1^0$1	0.5686	0.5686
00101 $_1^0$1	0.4768	0.4768	0001 $_1^0$1	0.6329	0.6329
001010 $_1^0$1	0.4980	0.4980	000111 $_1^0$1	0.5686	0.5686
001 $_1^0$1	0.5435	0.5435	00011 $_1^0$1	0.3822	0.3822
001110 $_1^0$1	0.4980	0.4980	000010 $_1^0$1	0.4589	0.4589
001111 $_1^0$1	0.4768	0.4768	00001 $_1^0$1	0.6662	0.6662
001111 $_1^0$1	0.3460	0.3460	000011 $_1^0$1	0.4589	0.4589
001101 $_1^0$1	0.4980	0.4980	000001 $_1^0$1	0.6804	0.6804

$F_1^p(w_\infty) = w_\infty$, which is the analog of the infinitely folded unstable manifold of the periodic orbit.

The growth rate $h(P)$ is expected to be the entropy $h_T(P)$ of orbit P, defined as the minimal topological entropy [8] of a map containing P [9]. Indeed, a piecewise linear map containing P with $(M_{ee'})$ as Markov transition matrix can be constructed and has entropy $h(P)$, thus $h_T(P) \leq h(P)$. Conversely, $h(P) \leq h_T(P)$, as $h(P)$ is the minimal growth rate of the geometric length of curves passing through periodic points P_i and cannot be larger than the topological entropy of a map containing P, which is the supremum of stretching rates over curves in the plane [15].

For a typical orbit, unlike in (4), there are paths in the F_1-invariant set that trigger a "squeezing" rule (2b), as, for example, $e_{16}e_{67} \rightarrow e_{17}$ for horseshoe orbit 0010111. Then $F_1(e_{16}e_{67}) \neq F_1(e_{16})F_1(e_{67})$ and the transition matrix cannot be used for entropy computations, although estimates can still be obtained by direct iteration. In all the examples we considered, enlarging the alphabet by recoding contracting paths as basis edges (e.g., $e_{167} \equiv e_{16}e_{67}$) and applying other recodings required for consistency allowed us to rewrite F_1 as an ordinary substitution like (4). For example, the induced return map for horseshoe orbit 0010111 can be rewritten as ($e_{ijk} \equiv e_{ij}e_{jk}$)

$$e_{14} \rightarrow e_{25}, \ e_{15} \rightarrow e_{257}e_{76}, \ e_{17} \rightarrow e_{257}e_{71}, \ e_{25} \rightarrow e_{37}e_{76},$$

$$e_{37} \rightarrow e_{41}, \ e_{67} \rightarrow e_{71}, \ e_{167} \rightarrow e_{25}e_{51}, \ e_{257} \rightarrow e_{37}e_{761}.$$

Besides e_{167}, basis path e_{257} was introduced because its image overlaps e_{167}. A transition matrix can then be obtained, with entropy $h(0010111) \sim 0.4768$.

For all 746 periodic orbits of the horseshoe map up to period 12, we have compared growth rate (5) with topological entropy obtained by the train-track algorithm [9,10,16]. As illustrated in Table II, we found *agreement to machine precision in each instance*. This strongly suggests that in 3D, our approach is equivalent to the train-track approach. Qualitative properties of chaos are also reproduced: the dynamics is deterministic (by construction), invertible, and the stretching and squeezing processes are described in a symmetrical way.

Remarkably, we note that while transformations (3) are *invertible*, the asymptotic dynamics is *singular*. Consider the itinerary $w_0 = F^3(e_{15}) = (41525153)$ in Table I, which is the shortest subpath of w_∞ visiting the four edges in (4). As Fig. 5(b) shows, the image $F_1(w_0) = (5251535152514) = (525153) + (35152514)$ consists of a subpath of w_0 concatenated with a reverse copy of w_0: *this path is folded onto itself by a singular one-dimensional map*. The same property holds for all subsequent iterates $F^m(e_{15})$, hence for the infinite word w_∞. This reflects that associated to an invertible return map (e.g., Hénon map), there exists an underlying lower-dimensional noninvertible map (e.g., logistic map) describing the dynamics along the unstable manifold, a keystone of the Birman-Williams construction [2,5]. Note that the symbolic name 00111 can be recovered directly from Fig. 5(b) using the usual coding for orbits of 1D maps. This makes the new formalism promising for using topological information to construct global symbolic codings as in [17]. How segments along w_0 are folded over each other and how neighboring cells are squeezed provide us with a combinatorial description of stretching and folding that could be used to determine the simplest template carrying the periodic orbit studied.

To conclude, we have proposed that orientation preservation is a more general formulation of determinism than nonintersection of trajectories. In three dimensions we find that enforcing it on a triangulation of periodic points induces a nontrivial dynamics on paths along periodic periodic points. More precisely, a path map F_1 is constructed by (i) following triangles advected by the flow as one rotates around the attractor, (ii) restoring orientation at each triangle inversion by exchanging opposing sides via transformations (2). When paths in the F_1-invariant set do not experience contraction, entropy is obtained from a transition matrix indicating how elementary edges in the invariant set are mapped among themselves. Otherwise, new basis paths must be introduced to account for contraction. A promising result is that despite its simplicity, this formalism numerically predicts the correct entropies for periodic orbits of the horseshoe map. Preliminary calculations also suggest that it leads to a combinatorial description of the folding of the invariant unstable manifold over itself, yielding information about the symbolic dynamics of the orbit. It now remains to prove the validity of the approcach in 3D and to try to extend it to higher dimensions.

[1] E. Ott, *Chaos in Dynamical Systems* (Cambridge University Press, Cambridge, 1993).

[2] R. Gilmore, Rev. Mod. Phys. **70**, 1455 (1998); R. Gilmore and M. Lefranc, *The Topology of Chaos* (Wiley, New York, 2002).

[3] G. B. Mindlin, X. J. Hou, H. G. Solari, R. Gilmore, and N. B. Tufillaro, Phys. Rev. Lett. **64**, 2350 (1990).

[4] G. B. Mindlin *et al.*, J. Nonlinear Sci. **1**, 147 (1991).

[5] J. S. Birman and R. F. Williams, Topology **22**, 47 (1983).

[6] G. Froyland, O. Junge, and G. Ochs, Physica D **154**, 68 (2001).

[7] S. Day, O. Junge and K. Mischaikow, SIAM J. Appl. Dyn. Syst. **2**, 117 (2004).

[8] P. Walters, *An Introduction to Ergodic Theory* (Springer, New York, 2000).

[9] P. Boyland, Topol. Appl. **58**, 223 (1994).

[10] M. Bestvina and M. Handel, Topology **34**, 109 (1995).

[11] A. Amon and M. Lefranc, Phys. Rev. Lett. **92**, 094101 (2004).

[12] J.-L. Thiffeault, Phys. Rev. Lett. **94**, 084502 (2005).

[13] G. B. Mindlin and H. G. Solari, Physica D **102**, 177 (1997).

[14] D. Sciamarella and G. B. Mindlin, Phys. Rev. Lett. **82**, 1450 (1999).

[15] S. E. Newhouse and T. Pignataro, J. Stat. Phys. **72**, 1331 (1993).

[16] T. Hall, TRAINS, software available from http://www.liv.ac.uk/maths/PURE/MIN_SET/CONTENT/members/ T_Hall.html.

[17] J. Plumecoq and M. Lefranc, Physica D **144**, 231 (2000).